

# Synchronization of Nonlinear Oscillators in an LTI Electrical Power Network

Brian B. Johnson, *Member, IEEE*, Sairaj V. Dhople, *Member, IEEE*, Abdullah O. Hamadeh, and Philip T. Krein, *Fellow, IEEE*

**Abstract**—Sufficient conditions are derived for the global asymptotic synchronization of a class of identical nonlinear oscillators coupled through a linear time-invariant network. In particular, we focus on systems where oscillators are connected to a common node through identical branch impedances. For such networks, it is shown that the synchronization condition is independent of the number of oscillators and the value of the load impedance connected to the common node. Theoretical findings are then leveraged to control a system of parallel single-phase voltage source inverters serving an impedance load in an islanded microgrid application. The ensuing paradigm: i) does not necessitate communication between inverters, ii) is independent of system load, and iii) facilitates a modular design approach because the synchronization condition is independent of the number of oscillators. We present both simulation and experimental case studies to validate the analytical results and demonstrate the proposed application.

**Index Terms**—Inverter control, microgrids, nonlinear oscillators, synchronization.

## I. INTRODUCTION

**S**YNCHRONIZATION of coupled oscillators is relevant to several research areas including neural processes, coherency in plasma physics, communications, and electronic circuits [1]–[7]. This paper presents a sufficient condition for global asymptotic synchronization of a class of identical nonlinear oscillators coupled through a linear time-invariant (LTI) network. In particular, symmetric networks composed of oscillators connected to a common node through identical branch impedances are examined. The synchronization condition is independent of: i) the load impedance (i.e., the impedance connected between the common node and electrical ground), and ii) the number of oscillators in the network. This result is used to formulate a control and analysis paradigm for

a decentralized power system composed of parallel voltage source inverters serving a passive electrical load.

Relevant to this work is a body of literature that has examined synchronization conditions for diffusively coupled oscillators using passivity theory [8]–[13]. For instance, in [13], the notions of passivity and incremental passivity [8]–[12] were used to establish synchronization conditions that were applied to the control of inverters as nonlinear oscillators in a power system. Passivity-based approaches require the formulation of a storage function, which can be difficult when the network contains energy-storage circuit elements such as inductors and capacitors. Since power networks are in general composed of a variety of LTI circuit elements (resistors, capacitors, inductors, and transformers), passivity-based approaches are difficult to apply in such systems. In this work, we use  $\mathcal{L}_2$  input-output stability methods, because they facilitate analysis in settings where storage functions are difficult to formulate. Our approach derives from previous work in [14]–[16] where  $\mathcal{L}_2$  methods were used to analyze synchronization in feedback systems. To prove synchronization, we reformulate the dynamics of the original system in a corresponding *differential system* based on signal differences. Stability of the differential system implies synchronization in the original system.

The application focus of this work is a decentralized control approach of power electronic inverters in a self-assembling and islanded ac microgrid. A *microgrid* is an electrical power system containing generation, storage, and loads that can operate independent of the bulk power system [17], [18]. Microgrids are an enabling technology for decentralized power systems since they provide a number of advantages including: increasing renewable integration, reducing transmission and distribution losses, and ensuring a reliable power supply to loads in mission-critical applications. Design objectives of microgrids are generally focused on minimizing communication [19], [20], maintaining stability [21]–[24], and ensuring that inverters share the load in proportion to their ratings [25], [26].

Inverters perform the key task of power delivery in an ac microgrid. With advances in digital control, they can be programmed to behave as controllable voltage sources [27]. In this work, we consider a particular islanded ac microgrid composed of a system of identical parallel single-phase inverters serving an impedance load. These inverters are controlled to behave as nonlinear oscillators that are designed to synchronize by applying the synchronization criteria described previously. The control scheme does not require communication between inverters (beyond the coupling inherently introduced by the elec-

Manuscript received February 28, 2013; revised June 14, 2013; accepted July 31, 2013. Date of publication January 02, 2014; date of current version February 21, 2014. The work of B. B. Johnson was supported in part by a National Science Foundation Graduate Research Fellowship and the Grainger Center for Electric Machinery and Electromechanics at the University of Illinois. The work of P. T. Krein was supported in part by the Global Climate and Energy Project at Stanford University. This paper was recommended by Associate Editor R. Sipahi.

B. B. Johnson is with the Power Systems Engineering Center at the National Renewable Energy Laboratory, Golden, CO 80401 USA (e-mail: brian.johnson@nrel.gov), but has written this article outside the scope of his employment.

S. V. Dhople is with the Department of Electrical and Computer Engineering at the University of Minnesota, Minneapolis, MN 55455 USA (e-mail: sdhople@umn.edu)

A. O. Hamadeh is with the Department of Mechanical Engineering, Massachusetts Institute of Technology, Cambridge, MA 02139 USA (email: ahamadeh@mit.edu).

P. T. Krein is with the Department of Electrical and Computer Engineering at the University of Illinois, Urbana, IL (email: krein@illinois.edu).

Color versions of one or more of the figures in this paper are available online at <http://ieeexplore.ieee.org>.

Digital Object Identifier 10.1109/TCSI.2013.2284180

trical network), is independent of the system load (because the synchronization condition is independent of load impedance), and facilitates a modular design approach (because the synchronization condition is independent of the number of oscillators). Also, the inverters share the load power demand with no supervisory control effort.

The state of the art method for inverter control in microgrids is *droop control*. This method requires no communication and is based on modulating the inverter output such that the frequency and voltage amplitude are inversely proportional to the real and reactive power output, respectively [20], [28], [29]. Recently, synchronization of droop-controlled inverters has been analyzed with equivalent Kuramoto-oscillator models, and sufficient conditions for convergence and stability have been obtained [30]–[32]. The oscillator-based method we propose differs from droop control in several respects. In particular, the proposed approach: i) does not require computation of the real and reactive power output, ii) demonstrates minimal deviations in system frequency from the rated value regardless of fluctuations in the load impedance, and iii) does not require an explicit frequency and amplitude command for the inverter ac output.

It is foreseen that the analytical results in this work will provide broad theoretical utility while outlining a compelling application to the control of inverters in microgrids. To summarize, the contributions of this work are as follows:

- 1) A sufficient global asymptotic synchronization condition is derived for a class of identical nonlinear oscillators connected to a common node through identical branch impedances.
- 2) It is shown that the synchronization condition is independent of the number of oscillators and the load impedance.
- 3) These results are applied towards the control of inverters in a single-phase microgrid to achieve a control and design paradigm that is robust (independent of load) and modular (independent of number of inverters).

The remainder of this paper is organized as follows: Notation and background material are presented in Section II. We describe the network topology of interest in Section III, and derive sufficient conditions for global asymptotic synchronization of the nonlinear oscillators in Section IV. In Section V, we formulate an oscillator model for inverter control and present simulations and experimental case studies. Concluding remarks are given in Section VI.

## II. PRELIMINARIES

For the  $N$ -tuple  $(u_1, \dots, u_N)$ , denote  $u = [u_1, \dots, u_N]^T$  to be the corresponding column vector, where  $(\cdot)^T$  indicates transposition. The  $N$ -dimensional column vectors of all ones and all zeros are denoted by  $\mathbf{1}$  and  $\mathbf{0}$ , respectively.

The Laplace transform of the continuous-time function  $f(t)$  is denoted by  $f(s)$ , where  $s = \rho + j\omega \in \mathbb{C}$ , and  $j = \sqrt{-1}$ . Transfer functions are denoted by lower-case  $z(s)$ , and transfer matrices are denoted by upper-case  $Z(s)$ .

The Euclidean norm of a real or complex vector,  $u$ , is denoted by  $\|u\|_2$  and is defined as

$$\|u\|_2 = \sqrt{u^* u}, \quad (1)$$

where  $(\cdot)^*$  indicates the conjugate transpose. For some continuous-time function  $u(t)$ ,  $u : [0, \infty) \rightarrow \mathbb{R}^N$ , the  $\mathcal{L}_2$  norm of  $u$  is defined as

$$\|u\|_{\mathcal{L}_2} = \sqrt{\int_0^{\infty} u(t)^T u(t) dt}, \quad (2)$$

and the space of piecewise-continuous and square-integrable functions where  $\|u\|_{\mathcal{L}_2} < \infty$  is denoted by  $\mathcal{L}_2$  [33]. A causal system,  $H$ , with input  $u$  and output  $y$ , is said to be *finite-gain  $\mathcal{L}_2$  stable* if there exist finite, non-negative constants,  $\gamma$  and  $\eta$ , such that

$$\|y\|_{\mathcal{L}_2} = \|H(u)\|_{\mathcal{L}_2} \leq \gamma \|u\|_{\mathcal{L}_2} + \eta, \quad \forall u \in \mathcal{L}_2. \quad (3)$$

The smallest value of  $\gamma$  for which there exists a  $\eta$  such that (3) is satisfied is called the  $\mathcal{L}_2$  gain of the system and is denoted by  $\gamma(H)$ . If  $H$  is a linear system and can be represented by the transfer function  $H(s)$ , it can be shown that the  $\mathcal{L}_2$  gain of  $H$  is equal to its  $\mathcal{H}$ -infinity norm, denoted by  $\|H\|_{\infty}$ , and defined as

$$\gamma(H) = \|H\|_{\infty} = \sup_{\omega \in \mathbb{R}} \frac{\|H(j\omega)u(j\omega)\|_2}{\|u(j\omega)\|_2}, \quad (4)$$

where  $\|u(j\omega)\|_2 = 1$ , provided that all poles of  $H(s)$  have strictly negative real parts [34]. Note that if  $H(s)$  is a single-input single-output transfer function then  $\gamma(H) = \|H\|_{\infty} = \sup_{\omega \in \mathbb{R}} \|H(j\omega)\|_2$ .

The electrical system of oscillators which interface to a common node corresponds to a network with all-to-all coupling. The *Laplacian* matrix of such a network is denoted as  $\Gamma \in \mathbb{R}^{N \times N}$ , and given by

$$\Gamma := NI_N - \mathbf{1}\mathbf{1}^T = \begin{bmatrix} N-1 & -1 & \cdots & -1 \\ -1 & N-1 & \cdots & -1 \\ \vdots & \vdots & \ddots & \vdots \\ -1 & -1 & \cdots & N-1 \end{bmatrix}. \quad (5)$$

This particular Laplacian has the following properties: i)  $\text{rank}(\Gamma) = N - 1$ , ii) the eigenvalues of  $\Gamma$  are denoted by  $\lambda_1 < \lambda_2 = \dots = \lambda_N$ , where  $\lambda_1 = 0$  and  $\lambda_j = N$  for  $j = 2, \dots, N$ , iii)  $\Gamma$  is symmetric with row and column sums equal to zero such that  $\Gamma\mathbf{1} = \Gamma^T\mathbf{1} = \mathbf{0}$ , iv) the eigenvector  $q_1$  (corresponding to  $\lambda_1 = 0$ ) is given by  $q_1 = (1/\sqrt{N})\mathbf{1}$ , and v)  $\Gamma$  can be diagonalized as  $Q\Lambda Q^T$ , where it follows that  $Q^{-1} = Q^T$  because  $\Gamma = \Gamma^T$ . See [15], [35], [36] for proofs and additional discussion.

A useful construct that will be employed to compare individual oscillator outputs with the average of all  $N$  oscillator outputs is the *projector matrix*,  $\Pi$ , defined as [9], [11], [15]

$$\Pi = I_N - \frac{1}{N}\mathbf{1}\mathbf{1}^T. \quad (6)$$

For some vector  $u \in \mathbb{R}^N$ , we will denote  $\tilde{u} = \Pi u$ , and refer to  $\tilde{u}$  as the corresponding *differential* vector (in previous work, see, e.g., [9], [11], [14]–[16], the quantity  $\tilde{u}$  was referred to as an incremental quantity). A causal system,  $H$ , with input  $u$  and

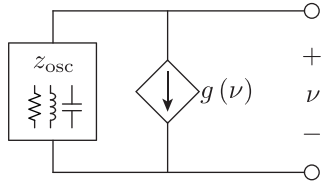


Fig. 1. The oscillator model in this work is composed of a linear subsystem,  $z_{osc}(s)$ , and a nonlinear voltage-dependent current source,  $g(v)$ .

output  $y$ , is said to be *differentially finite-gain  $\mathcal{L}_2$  stable* if there exist finite, non-negative constants,  $\tilde{\gamma}$  and  $\tilde{\eta}$ , such that

$$\|\tilde{y}\|_{\mathcal{L}_2} \leq \tilde{\gamma}\|\tilde{u}\|_{\mathcal{L}_2} + \tilde{\eta}, \quad \forall \tilde{u} \in \mathcal{L}_2, \quad (7)$$

where  $\tilde{y} = \Pi y$ . The smallest value of  $\tilde{\gamma}$  for which there exists a  $\tilde{\eta}$  such that (7) is satisfied is called the *differential  $\mathcal{L}_2$  gain* of the system and is denoted by  $\tilde{\gamma}(H)$ .

### III. SYSTEM OF COUPLED OSCILLATORS

In this section, a system of  $N$  nonlinear coupled oscillators is introduced. We consider a network topology where all oscillators are connected to a common node through identical impedances. A corresponding differential system is then developed to facilitate synchronization analysis.

Our interest in this particular topology stems from the fact that inverters in a microgrid are often connected in parallel to serve a load [20], [37]. In the forthcoming section, we will show that the synchronization condition for this network is independent of the number of oscillators and the load impedance. This is a useful result, because it implies the system can be designed without *a priori* information of the load parameters and number of inverters.

#### A. System Description

As shown in Fig. 1, the electrical oscillator under consideration has: i) a linear subsystem composed of passive circuit elements with impedance  $z_{osc}(s)$ , and ii) a nonlinear voltage-dependent current source  $g(\cdot)$ . We will require that  $g(\cdot)$  be continuous and differentiable, and additionally impose

$$\sigma := \sup_{v \in \mathbb{R}} \left| \frac{d}{dv} g(v) \right| < \infty. \quad (8)$$

Fig. 2 depicts an electrical network of  $N$  such oscillators connected to a common (load) node through identical branch impedances,  $z_{net}(s)$  (which may contain any combination of linear circuit elements). The  $N$  oscillators deliver power to a passive LTI load,  $z_{load}(s)$ , which is connected at the common node. The coupling between oscillators is captured by

$$i(s) = Y(s)v(s), \quad (9)$$

where  $i(s) = [i_1(s), \dots, i_N(s)]^T$  is the vector of oscillator output currents,  $v(s) = [v_1(s), \dots, v_N(s)]^T$  is the vector of oscillator terminal voltages, and  $Y(s)$  is the network admittance matrix.

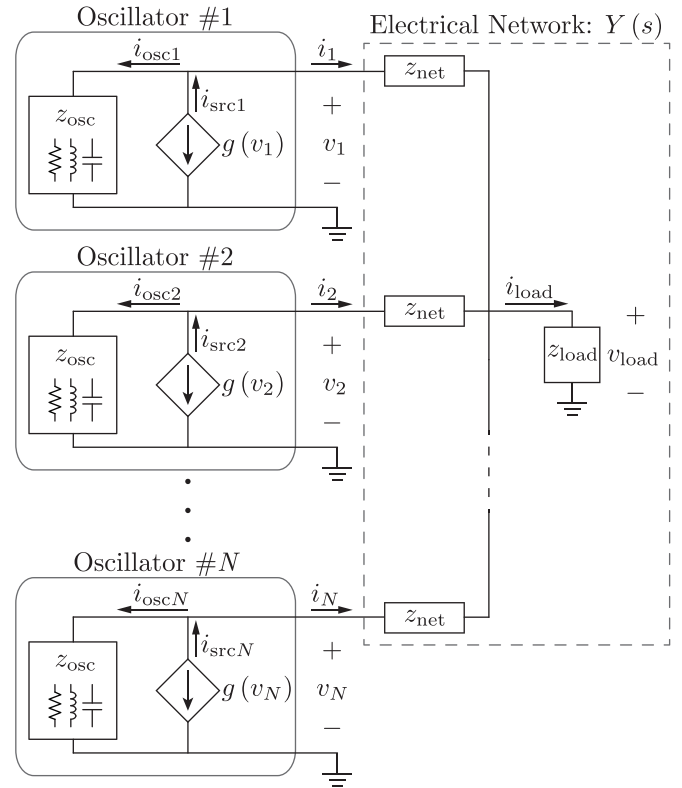


Fig. 2.  $N$  parallel oscillators interconnected through an LTI electrical network containing a passive impedance load.

A closed-form expression for  $Y(s)$  will now be derived. Towards this end, notice from Fig. 2 that the  $j^{\text{th}}$  oscillator output current is given by

$$i_j(s) = \frac{1}{z_{net}(s)}(v_j(s) - v_{load}(s)), \quad (10)$$

where the load voltage,  $v_{load}(s)$ , can be expressed as

$$v_{load}(s) = z_{load}(s) \sum_{k=1}^N i_k(s). \quad (11)$$

Substituting (11) in (10) yields

$$i_j(s) = \frac{1}{z_{net}(s)} \left( v_j(s) - z_{load}(s) \sum_{k=1}^N i_k(s) \right), \quad (12)$$

from which  $v_j(s)$  can be isolated to obtain

$$v_j(s) = z_{net}(s)i_j(s) + z_{load}(s) \sum_{k=1}^N i_k(s). \quad (13)$$

Collecting all terminal voltages,

$$v(s) = (z_{net}(s)I_N + z_{load}(s)\mathbf{1}\mathbf{1}^T)i(s). \quad (14)$$

Comparing (14) with (9) indicates

$$Y^{-1}(s) = z_{net}(s)I_N + z_{load}(s)\mathbf{1}\mathbf{1}^T. \quad (15)$$

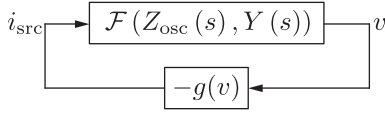


Fig. 3. Representation of coupled oscillator system. The linear and nonlinear portions of the system are compartmentalized in  $\mathcal{F}(\cdot, \cdot)$  and  $g(\cdot)$ , respectively.

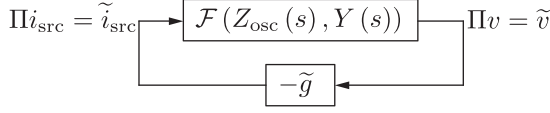


Fig. 4. Block-diagram representation of the corresponding differential system. The linear and nonlinear portions of the system are compartmentalized in  $\mathcal{F}(\cdot, \cdot)$  and  $\tilde{g}$ , respectively.

The above expression can be inverted to obtain

$$Y(s) = \alpha(s)I_N + \beta(s)\Gamma, \quad (16)$$

where  $\alpha(s), \beta(s) \in \mathbb{C}$  are given by

$$\begin{cases} \alpha(s) = (z_{\text{net}}(s) + Nz_{\text{load}}(s))^{-1} =: z_{\text{eq}}^{-1}(s), \\ \beta(s) = z_{\text{load}}(s)(z_{\text{net}}(s)z_{\text{eq}}(s))^{-1}. \end{cases} \quad (17)$$

See Appendix A for a proof of the above result. Using the expressions for  $Y(s)$  in (16)–(17), it is possible to redraw the microgrid network in Fig. 2 as another equivalent network containing admittances  $\alpha(s)$  and  $\beta(s)$ .

We now seek a representation of the system in Fig. 2, where the linear and nonlinear portions of the system are clearly differentiated. Towards this end, first note that the terminal voltage of the  $j^{\text{th}}$  oscillator,  $v_j(s)$ , can be expressed as

$$v_j(s) = z_{\text{osc}}(s)(i_{\text{src}j}(s) - i_j(s)). \quad (18)$$

Writing all  $v_j$ 's in matrix form yields

$$\begin{aligned} v(s) &= Z_{\text{osc}}(s)(i_{\text{src}}(s) - i(s)) \\ &= Z_{\text{osc}}(s)i_{\text{src}}(s) - Z_{\text{osc}}(s)Y(s)v(s), \end{aligned} \quad (19)$$

where  $Z_{\text{osc}}(s) = z_{\text{osc}}(s) \cdot I_N \in \mathbb{C}^{N \times N}$ ,  $i_{\text{src}}(s) = [i_{\text{src}1}(s), \dots, i_{\text{src}N}(s)]^T$ , and in the second line of (19), we have substituted  $i(s) = Y(s)v(s)$  from (9). We can isolate  $v(s)$  from (19) as follows:

$$\begin{aligned} v(s) &= (I_N + Z_{\text{osc}}(s)Y(s))^{-1}Z_{\text{osc}}(s)i_{\text{src}}(s) \\ &= \mathcal{F}(Z_{\text{osc}}(s), Y(s))i_{\text{src}}(s), \end{aligned} \quad (20)$$

where  $\mathcal{F} : \mathbb{C}^{N \times N} \times \mathbb{C}^{N \times N} \rightarrow \mathbb{C}^{N \times N}$  is the *linear fractional transformation*, and represents  $Z_{\text{osc}}(s)$  in negative feedback with  $Y(s)$  [38]. In general, for some  $A, B$  of appropriate dimension, the linear fractional transformation is defined as

$$\mathcal{F}(A, B) := (I_N + AB)^{-1}A. \quad (21)$$

Using (20), the system of coupled oscillators admits the compact block-diagram representation in Fig. 3. The linear and nonlinear portions of the system are clearly compartmentalized by

$\mathcal{F}(Z_{\text{osc}}(s), Y(s))$  and  $g(v) := [g(v_1), \dots, g(v_N)]^T$ , respectively.

### B. Corresponding Differential System Description

Global asymptotic synchronization of the coupled oscillator system in Section III-A corresponds to the condition

$$\lim_{t \rightarrow \infty} v_j(t) - v_k(t) = 0 \quad \forall j, k = 1, \dots, N. \quad (22)$$

For ease of analysis, we will find it useful to transform to a coordinate system based on signal differences. Towards this end, we employ the projector matrix in (6), noting that [14], [15]

$$\tilde{v}(t)^T \tilde{v}(t) = (\Pi v(t))^T (\Pi v(t)) = \frac{1}{2N} \sum_{j=1}^N \sum_{k=1}^N (v_j(t) - v_k(t))^2. \quad (23)$$

Therefore, it is evident that the synchronization condition in (22) is equivalent to requiring  $\tilde{v}(t) = \Pi v(t) \rightarrow \mathbf{0}$  as  $t \rightarrow \infty$ . Henceforth, we will refer to the system where all vectors are transformed by the projector matrix as the corresponding *differential system*.

We will now use the dynamics of the original system to construct the corresponding differential system, the stability of which will imply synchronization in the sense of (22). Towards this end, the differential terminal-voltage vector,  $\tilde{v}(s)$ , can be expressed as

$$\begin{aligned} \tilde{v}(s) &= \Pi v(s) = \Pi(Z_{\text{osc}}(s)(i_{\text{src}}(s) - i(s))) \\ &= Z_{\text{osc}}(s)(\Pi i_{\text{src}}(s) - \Pi Y(s)v(s)) \\ &= Z_{\text{osc}}(s)(\tilde{i}_{\text{src}}(s) - Y(s)\tilde{v}(s)), \end{aligned} \quad (24)$$

where in the first line, we have substituted for  $v(s)$  from (19); in the second line, we have used the relation  $i(s) = Y(s)v(s)$  from (9) and the fact that  $\Pi Z_{\text{osc}}(s) = \Pi z_{\text{osc}}(s)I_N = z_{\text{osc}}(s)I_N\Pi = Z_{\text{osc}}(s)\Pi$ ; and in the last line, we have used the property that the projector and admittance matrices commute, i.e.,  $\Pi Y(s) = Y(s)\Pi$  (this follows straightforwardly from the fact that  $\Gamma\Pi = \Pi\Gamma$ ). We can now isolate  $\tilde{v}(s)$  in (24) as follows:

$$\begin{aligned} \tilde{v}(s) &= (I_N + Z_{\text{osc}}(s)Y(s))^{-1}Z_{\text{osc}}(s)\tilde{i}_{\text{src}}(s) \\ &= \mathcal{F}(Z_{\text{osc}}(s), Y(s))\tilde{i}_{\text{src}}(s). \end{aligned} \quad (25)$$

Notice the similarity between (25) and (20); i.e., the linear fractional transformation also maps  $\tilde{i}_{\text{src}}(s)$  to  $\tilde{v}(s)$ .

Finally, we can define a map  $\tilde{g}$  that captures the impact of  $g(v)$  in the corresponding differential system as follows:

$$\tilde{g} : \tilde{v} \rightarrow -\tilde{i}_{\text{src}}. \quad (26)$$

We now have a complete description of the corresponding differential system. In particular, this system admits the block-diagram representation in Fig. 4, where, as in Fig. 3, the linear and nonlinear subsystems are compartmentalized using  $\mathcal{F}(\cdot, \cdot)$  and  $\tilde{g}$ , respectively.

#### IV. GLOBAL ASYMPTOTIC SYNCHRONIZATION

In this section, we derive a sufficient condition that ensures global asymptotic synchronization in the sense of (22) for the system of oscillators described in Section III-A.

First, we present a lemma that will establish an upper bound on the differential  $\mathcal{L}_2$  gain of  $g$ .

*Lemma 1:* The differential  $\mathcal{L}_2$  gain of  $g$  is finite and upper bounded by  $\sigma$ :

$$\tilde{\gamma}(g) \leq \sigma = \sup_{\nu \in \mathbb{R}} \left| \frac{d}{d\nu} g(\nu) \right| < \infty. \quad (27)$$

*Proof:* By definition of  $\sigma$ , for any pair of terminal voltages  $v_j$  and  $v_k$ , and the corresponding currents  $i_{srcj}$  and  $i_{srck}$ , where  $j, k \in \{1, \dots, N\}$ , the mean-value theorem [34] can be applied to give

$$\begin{aligned} \sigma &\geq \frac{|i_{srcj}(t) - i_{srck}(t)|}{|v_j(t) - v_k(t)|} \\ \Rightarrow \sigma^2 (v_j(t) - v_k(t))^2 &\geq (i_{srcj}(t) - i_{srck}(t))^2. \end{aligned} \quad (28)$$

Summing over all indices,  $j, k \in \{1, \dots, N\}$ , we arrive at

$$\sigma^2 \sum_{j=1}^N \sum_{k=1}^N (v_j(t) - v_k(t))^2 \geq \sum_{j=1}^N \sum_{k=1}^N (i_{srcj}(t) - i_{srck}(t))^2, \quad (29)$$

which can be rearranged and simplified as

$$\sigma \geq \sqrt{\frac{\sum_{j=1}^N \sum_{k=1}^N (i_{srcj}(t) - i_{srck}(t))^2}{\sum_{j=1}^N \sum_{k=1}^N (v_j(t) - v_k(t))^2}}. \quad (30)$$

Since (30) holds for any set of terminal voltages, we obtain

$$\sigma \geq \sup_{v \in \mathbb{R}^N} \sqrt{\frac{\frac{1}{2N} \sum_{j=1}^N \sum_{k=1}^N (i_{srcj}(t) - i_{srck}(t))^2}{\frac{1}{2N} \sum_{j=1}^N \sum_{k=1}^N (v_j(t) - v_k(t))^2}}, \quad (31)$$

which can be rewritten compactly using the projector-matrix notation in (23) as follows:

$$\sigma \geq \sup_{v \in \mathbb{R}^N} \sqrt{\frac{\tilde{i}_{src}(t)^T \tilde{i}_{src}(t)}{\tilde{v}(t)^T \tilde{v}(t)}}. \quad (32)$$

By definition of the differential  $\mathcal{L}_2$  gain, we have

$$\begin{aligned} \tilde{\gamma}(g) &= \sup_{v \in \mathbb{R}^N} \frac{\|\tilde{i}_{src}\|_{\mathcal{L}_2}}{\|\tilde{v}\|_{\mathcal{L}_2}} \\ &= \sup_{v \in \mathbb{R}^N} \frac{\sqrt{\int_0^\infty \tilde{i}_{src}(t)^T \tilde{i}_{src}(t) dt}}{\sqrt{\int_0^\infty \tilde{v}(t)^T \tilde{v}(t) dt}}. \end{aligned} \quad (33)$$

Applying (32) in the definition above, we attain

$$\tilde{\gamma}(g) \leq \sup_{v \in \mathbb{R}^N} \sqrt{\frac{\sigma^2 \int_0^\infty \tilde{v}(t)^T \tilde{v}(t) dt}{\int_0^\infty \tilde{v}(t)^T \tilde{v}(t) dt}} = \sigma < \infty, \quad (34)$$

which completes the proof.  $\blacksquare$

We now prove the main result of this work: a sufficient condition for global asymptotic synchronization in the network of oscillators described in Section III-A.

*Theorem 1:* The network of  $N$  oscillators coupled through (9) with the admittance matrix as defined in (16)–(17), synchronizes in the sense of (22), if

$$\sup_{\omega \in \mathbb{R}} \left\| \frac{z_{net}(j\omega) z_{osc}(j\omega)}{z_{net}(j\omega) + z_{osc}(j\omega)} \right\|_2 \sigma < 1. \quad (35)$$

*Proof:* Consider the block-diagram of the differential system in Fig. 4. Denoting the differential  $\mathcal{L}_2$  gain of the linear fractional transformation by  $\tilde{\gamma}(\mathcal{F}(Z_{osc}(s), Y(s)))$ , we have

$$\|\tilde{v}\|_{\mathcal{L}_2} \leq \tilde{\gamma}(\mathcal{F}(Z_{osc}(s), Y(s))) \|\tilde{i}_{src}\|_{\mathcal{L}_2} + \eta, \quad (36)$$

for some non-negative  $\eta$ . From Lemma 1, we also have

$$\|\tilde{i}_{src}\|_{\mathcal{L}_2} \leq \sigma \|\tilde{v}\|_{\mathcal{L}_2}. \quad (37)$$

Combining (36) and (37), we arrive at

$$\|\tilde{v}\|_{\mathcal{L}_2} \leq \tilde{\gamma}(\mathcal{F}(Z_{osc}(s), Y(s))) \sigma \|\tilde{v}\|_{\mathcal{L}_2} + \eta. \quad (38)$$

Let us assume that

$$\tilde{\gamma}(\mathcal{F}(Z_{osc}(s), Y(s))) \sigma < 1. \quad (39)$$

Isolating  $\|\tilde{v}\|_{\mathcal{L}_2}$  from (38), we can write

$$\|\tilde{v}\|_{\mathcal{L}_2} \leq \frac{\eta}{1 - \tilde{\gamma}(\mathcal{F}(Z_{osc}(s), C(s))) \sigma}, \quad (40)$$

which implies that  $\tilde{v} \in \mathcal{L}_2$ . It follows from Barbalat's lemma [14]–[16], [34] that

$$\begin{aligned} \lim_{t \rightarrow \infty} \tilde{v}(t) = \mathbf{0} &\Rightarrow \lim_{t \rightarrow \infty} v_j(t) - v_k(t) = 0 \\ &\quad \forall j, k = 1, \dots, N. \end{aligned} \quad (41)$$

That is, if the system of oscillators satisfies the condition in (39), global asymptotic synchronization can be guaranteed.

We will now derive the result in (35) by showing  $\tilde{\gamma}(\mathcal{F}(Z_{osc}(s), Y(s))) = \|(z_{net}(j\omega) z_{osc}(j\omega)) / (z_{net}(j\omega) + z_{osc}(j\omega))\|_\infty$ . From the definition of the linear fractional transformation in (21) and the general form of the admittance matrix in (16), note that

$$\begin{aligned} \mathcal{F}(Z_{osc}(s), Y(s)) &= (I_N + Z_{osc}(s)Y(s))^{-1} Z_{osc}(s) \\ &= (I_N + Z_{osc}(s)(\alpha(s)I_N + \beta(s)\Gamma))^{-1} Z_{osc}(s) \\ &= \left( I_N + \frac{z_{osc}(s)}{1 + \alpha(s)z_{osc}(s)} \beta(s)\Gamma \right)^{-1} \frac{z_{osc}(s)I_N}{1 + \alpha(s)z_{osc}(s)} \\ &= \mathcal{F}(\zeta(s)I_N, \beta(s)\Gamma), \end{aligned} \quad (42)$$

where we have defined

$$\zeta(s) := \frac{z_{osc}(s)}{1 + \alpha(s)z_{osc}(s)}, \quad (43)$$

with  $\alpha(s)$  and  $\beta(s)$  given in (17). Now, by definition of the differential  $\mathcal{L}_2$  gain of the linear fractional transformation, we can express

$$\begin{aligned} \tilde{\gamma}(\mathcal{F}(Z_{\text{osc}}(s), Y(s))) &= \tilde{\gamma}(\mathcal{F}(\zeta(s)I_N, \beta(s)\Gamma)) \\ &= \sup_{\omega \in \mathbb{R}} \frac{\|\mathcal{F}(\zeta(s)I_N, \beta(s)\Gamma)\tilde{i}_{\text{src}}(j\omega)\|_2}{\|\tilde{i}_{\text{src}}(j\omega)\|_2} \\ &= \sup_{\omega \in \mathbb{R}} \frac{\|(I_N + \zeta(j\omega)\beta(j\omega)\Gamma)^{-1}\zeta(j\omega)\tilde{i}_{\text{src}}(j\omega)\|_2}{\|\tilde{i}_{\text{src}}(j\omega)\|_2} \\ &= \sup_{\omega \in \mathbb{R}} \frac{\|Q(I_N + \zeta(j\omega)\beta(j\omega)\Lambda)^{-1}\zeta(j\omega)Q^T\tilde{i}_{\text{src}}(j\omega)\|_2}{\|Q^T\tilde{i}_{\text{src}}(j\omega)\|_2}, \end{aligned} \quad (44)$$

where, we have diagonalized  $\Gamma = Q\Lambda Q^T$  and recognized that  $QQ^T = I_N$ . We will now make two key observations to simplify (44):

- i) The first column of  $Q$  is given by  $q_1 = (1/\sqrt{N})\mathbf{1}$ . Furthermore,  $\mathbf{1}^T\Pi = \mathbf{0}^T$ . Therefore, the vector  $Q^T\tilde{i}_{\text{src}}(s) = Q^T\Pi i_{\text{src}}(s)$  is given by

$$Q^T\tilde{i}_{\text{src}}(s) = Q^T\Pi i_{\text{src}}(s) = [0, D(s)]^T, \quad (45)$$

where  $D(s) \in \mathbb{C}^{N-1 \times 1}$  is made up of the non-zero elements of  $Q^T\Pi i_{\text{src}}(s)$ .

- ii) Denote the diagonal matrix with entries made up of the non-zero eigenvalues of  $\Gamma$  by  $\Lambda_{N-1}$ . By definition of  $\Gamma$  in Section II, we see that  $\Lambda_{N-1} = N \cdot I_{N-1} \in \mathbb{R}^{N-1 \times N-1}$ .

Using the two observations highlighted above, we can simplify (44) as follows:

$$\begin{aligned} \tilde{\gamma}(\mathcal{F}(\zeta(s)I_N, \beta(s)\Gamma)) &= \sup_{\omega \in \mathbb{R}} \frac{\|(I_{N-1} + \zeta(j\omega)\beta(j\omega)\Lambda_{N-1})^{-1}\zeta(j\omega)D(j\omega)\|_2}{\|D(j\omega)\|_2} \\ &= \sup_{\omega \in \mathbb{R}} \left( \frac{1}{D^T(j\omega)D(j\omega)} \frac{\zeta^2(j\omega)D^T(j\omega)D(j\omega)}{(1 + \zeta(j\omega)\beta(j\omega)N)^2} \right)^{\frac{1}{2}} \\ &= \sup_{\omega \in \mathbb{R}} (1 + \zeta(j\omega)\beta(j\omega)N)^{-1}\zeta(j\omega) \\ &= \|\mathcal{F}(\zeta(s), \beta(s)N)\|_{\infty}. \end{aligned} \quad (46)$$

Finally, for the  $\alpha(s)$  and  $\beta(s)$  in (17), we can simplify  $\mathcal{F}(\zeta(s), \beta(s)N)$  as follows:

$$\begin{aligned} \mathcal{F}(\zeta(s), \beta(s)N) &= (1 + \zeta(s)\beta(s)N)^{-1}\zeta(s) \\ &= \frac{z_{\text{osc}}z_{\text{eq}}(z_{\text{osc}} + z_{\text{eq}})^{-1}}{1 + z_{\text{osc}}z_{\text{eq}}(z_{\text{osc}} + z_{\text{eq}})z_{\text{load}}z_{\text{net}}^{-1}z_{\text{eq}}^{-1}N} \\ &= \frac{z_{\text{osc}}}{z_{\text{eq}}^{-1}(z_{\text{osc}} + z_{\text{eq}}) + z_{\text{osc}}z_{\text{eq}}^{-1}z_{\text{load}}z_{\text{net}}^{-1}N} \\ &= \frac{z_{\text{osc}}}{1 + z_{\text{osc}}z_{\text{eq}}^{-1}(1 + z_{\text{load}}z_{\text{net}}^{-1}N)} \\ &= \frac{z_{\text{osc}}}{1 + z_{\text{osc}}z_{\text{eq}}^{-1}(z_{\text{eq}}z_{\text{net}}^{-1})} = \frac{z_{\text{osc}}(s)z_{\text{net}}(s)}{z_{\text{net}}(s) + z_{\text{osc}}(s)}, \end{aligned} \quad (47)$$

which completes the proof.  $\blacksquare$

The condition for synchronization in (35) is independent of the number of oscillators,  $N$ , and the load impedance,  $z_{\text{load}}(s)$ .

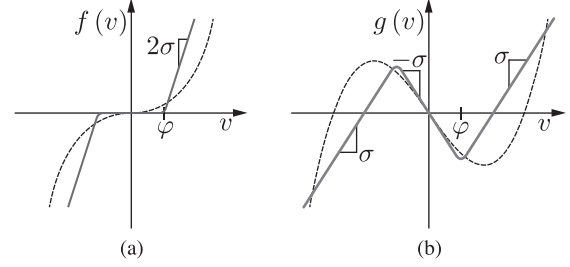


Fig. 5. The functions (a) $f(v)$  and (b) $g(v)$  illustrated for the Van der Pol (dashed lines) and dead-zone (solid lines) oscillators. For the dead-zone oscillator,  $\sup_{v \in \mathbb{R}} |dg(v)/dv| = \sigma$ .

It depends only on the impedance of the parallel combination of  $z_{\text{osc}}(s)$  and  $z_{\text{net}}(s)$ .

In Appendix C, we discuss how the results presented above can be extended to the case where the oscillators are not homogeneous, and the network branch impedances are not identical.

## V. CASE STUDIES

The proposed microgrid control is grounded on programming inverters to emulate nonlinear oscillators. Towards that end, we first present the particular oscillator model which will form the basis of the inverter control. Next, we describe the parameter selection approach to ensure the inverters synchronize while ensuring the load voltage and system frequency meet performance objectives. We also describe how the controller can be implemented on a digital platform. Finally, simulation and experimental case studies that demonstrate the analytical results as applied to inverters in a microgrid are presented.

### A. Nonlinear Oscillator Description

In this work, we utilize a *dead-zone oscillator*, in which the nonlinear voltage-dependent current source is given by

$$g(v) = f(v) - \sigma v, \quad (48)$$

where  $f(\cdot)$  is a continuous, differentiable dead-zone function with slope  $2\sigma$ , and  $f(v) \equiv 0$  for  $v \in (-\varphi, +\varphi)$ . Furthermore, the linear subsystem is a parallel  $RLC$  circuit:

$$z_{\text{osc}}(s) = R \| sL \| (sC)^{-1}. \quad (49)$$

The functions  $f(v)$  and  $g(v)$  are illustrated in Fig. 5.<sup>1</sup> The terminal voltage of the dead-zone oscillator satisfies

$$LC \frac{d^2v}{dt^2} + L \left( \frac{df(v)}{dv} + \frac{1}{R} - \sigma \right) \frac{dv}{dt} + v = 0. \quad (50)$$

The existence of a stable and unique limit cycle can be determined with the aid of Liénard's Theorem, which is stated below.

*Theorem 2:* (Liénard's Theorem [4]) Consider the system

$$\ddot{v} + r(v)\dot{v} + m(v) = 0, \quad (51)$$

<sup>1</sup>The proposed dead-zone oscillator is very similar to the well-known Van der Pol oscillator. To facilitate comparison, the functions  $f(v)$  and  $g(v)$  for the Van-der-Pol oscillator are superimposed in Fig. 5.

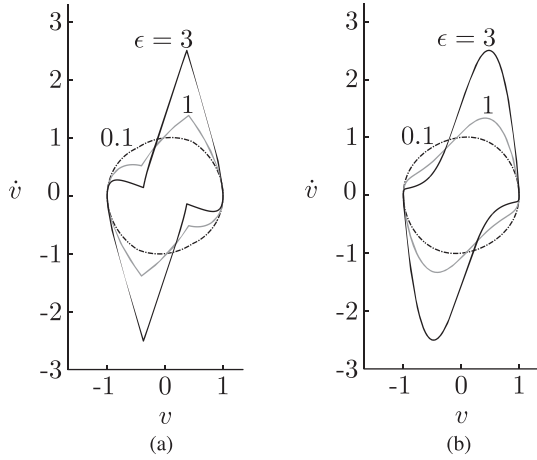


Fig. 6. Phase plot of steady-state limit cycles in the (a) dead-zone and (b) Van der Pol oscillators for varying  $\epsilon = \sqrt{L/C}(\sigma - (1/R))$ .

where  $v : [0, \infty) \rightarrow \mathbb{R}$  and  $r(v), m(v) : \mathbb{R} \rightarrow \mathbb{R}$  are differentiable, even and odd functions, respectively. Define

$$R(v) := \int_0^v r(\tau) d\tau. \quad (52)$$

The system in (51) has a unique and stable limit cycle if: i)  $m(v) > 0 \forall v > 0$ , ii)  $R(v)$  has one positive zero for some  $v = p$ , iii)  $R(v) < 0$  when  $0 < v < p$ , and iv)  $R(v)$  monotonically increases for  $v > p$  and  $\lim_{v \rightarrow \infty} R(v) = \infty$ .

We can rewrite (50) by expressing the derivatives of  $v$  with respect to  $\xi := t/\sqrt{LC}$  to yield

$$\ddot{v} + \sqrt{\frac{L}{C}} \left( \frac{df(v)}{dv} + \frac{1}{R} - \sigma \right) \dot{v} + v = 0, \quad (53)$$

which is of the form in (51), with

$$\begin{cases} m(v) = v, \\ r(v) = \sqrt{\frac{L}{C}} \left( \frac{df(v)}{dv} + \frac{1}{R} - \sigma \right). \end{cases} \quad (54)$$

For the case  $\sigma > 1/R$ , it is easy to see that  $m(v)$ ,  $r(v)$ , and  $R(v)$  satisfy the conditions in Liénard's theorem, implying that the dead-zone oscillator has a stable and unique limit cycle. The steady-state limit cycles of the dead-zone oscillator for different values of  $\epsilon = \sqrt{L/C}(\sigma - (1/R))$  are plotted in Fig. 6(a). For comparison, the limit cycles of the Van der Pol oscillator for the same set of parameters are shown in Fig. 6(b). When  $\epsilon \ll 1$ , it can be shown that the steady-state oscillation will have a frequency approximately equal to  $1/\sqrt{LC}$  [34], and as shown in Fig. 6(a), the limit cycle is approximately a circle in the current-voltage space.

### B. Parameter Selection and Controller Implementation

In all the case studies, we consider a network with the topology in Fig. 2. The network branch impedance is given by  $z_{\text{net}}(s) = sL_{\text{net}} + R_{\text{net}}$ , where  $L_{\text{net}}$  and  $R_{\text{net}}$  equal the series combination of the line and inverter-output-filter inductance and resistance, respectively (the inverter output-filter inductance

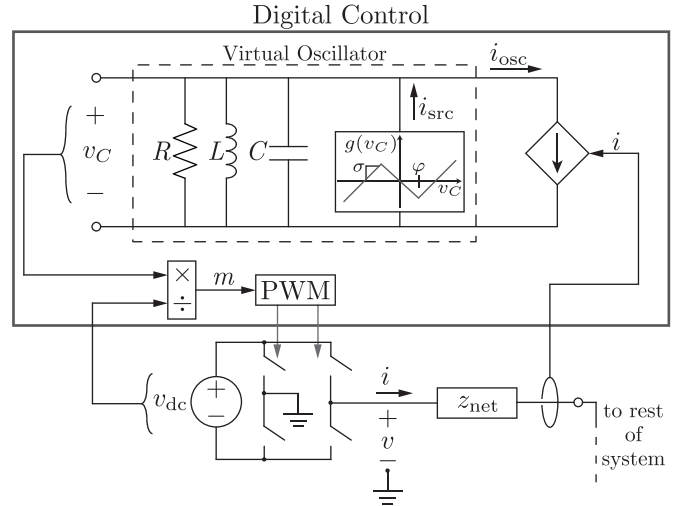


Fig. 7. Controller implementation that ensures the H-bridge inverter emulates the behavior of the nonlinear dead-zone oscillator.

reduces harmonics which arise due to switching [27]). Finally, we assume the load is resistive such that  $z_{\text{load}}(s) = R_{\text{load}}$  (note that our result applies in general to any passive LTI load). For this system, the linear fractional transformation is given by

$$\mathcal{F}(z_{\text{osc}}(s), z_{\text{net}}^{-1}(s)) = \frac{a_2 s^2 + a_1 s}{b_3 s^3 + b_2 s^2 + b_1 s + b_0}, \quad (55)$$

where  $a_2 = L_{\text{net}}$ ,  $a_1 = R_{\text{net}}$ ,  $b_3 = L_{\text{net}}C$ ,  $b_2 = (L_{\text{net}}/R) + R_{\text{net}}C$ ,  $b_1 = (L_{\text{net}}/L) + (R_{\text{net}}/R) + 1$ , and  $b_0 = R_{\text{net}}/L$ .

The design objective is to guarantee that the inverters synchronize their voltage outputs, and oscillate at the desired frequency. Additionally, in steady-state we will require  $v_{\text{load}}$  to stay within  $\pm 5\%$  of the rated voltage across the entire load range (no-load to maximum rated load). For a given filter impedance,  $z_{\text{net}}(s)$ , the above design objective can be satisfied by proper selection of the oscillator linear- and nonlinear-subsystem parameters including:  $R$ ,  $L$ ,  $C$ ,  $\sigma$ , and  $\varphi$ .

To ensure oscillations at the rated system frequency,  $\omega_{\text{rated}}$ , the values of  $R$ ,  $L$ , and  $C$  must be selected such that  $R > 1/\sigma$ ,  $LC = 1/\omega_{\text{rated}}^2$ . Further, we must ensure that  $\epsilon = \sqrt{L/C}(\sigma - 1/R)$  is minimized to guarantee that the terminal inverter voltages are sinusoidal, and  $\sigma$  is picked so that  $\|\mathcal{F}(z_{\text{osc}}(j\omega), z_{\text{net}}^{-1}(j\omega))\|_{\infty} \sigma < 1$  to guarantee synchronization. The value of  $\varphi$  can be tuned with an open-circuit test to ensure that the inverter output voltage is no more than the peak allowed load voltage.

Fig. 7 illustrates how the oscillator-based controller is implemented for a single-phase H-bridge inverter. As shown, the terminal current of the inverter is measured, and extracted from the virtual oscillator. The modulation signal,  $m$ , is the scaled oscillator voltage. The inverter switching signals are generated by comparing the modulation signal with a triangle carrier waveform [27]. With the proposed method, the inverter emulates the dynamics of the nonlinear dead-zone oscillator. Discretization of the virtual oscillator differential equations is straightforward, and the proposed controller can be implemented on a standard microcontroller.

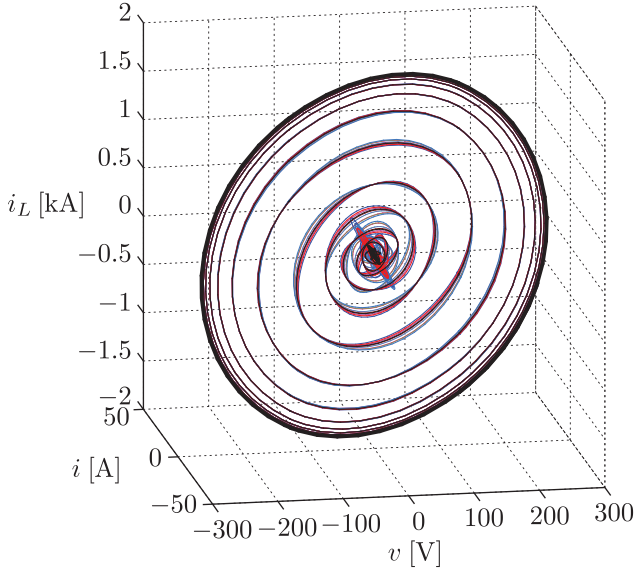


Fig. 8. Evolution of oscillator state variables during startup in the presence of a load. Waveforms for only 10 inverters out of 100 simulated are shown for clarity.

### C. Simulation and Experimental Results

We now present simulation and experimental results to validate the analytical methods in a microgrid application. In particular, we demonstrate that a system of inverters controlled as deadzone oscillators satisfying (35) synchronize and deliver power to a load.

In case studies I and II, a microgrid consisting of 100 parallel inverters which are each rated for 10 kW was simulated. The RMS voltage and frequency ratings of the system are 220 V and 60 Hz, respectively, and the maximum load power is 1 MW. In case study III, we provide experimental results for a laboratory prototype which consists of three parallel inverters. The system parameters used in the case studies are summarized in Table I in Appendix B.

*Case Study I (Simulation):* Substituting the parameter values from Table I into (55), it can be shown that  $\|\mathcal{F}(z_{osc}(j\omega), z_{net}^{-1}(j\omega))\|_{\infty} \sigma = 0.77 < 1$ , which guarantees synchronization. At  $t = 0$ , all currents are zero and the oscillator capacitor voltages are randomly selected between  $\pm 10$  V. Initially, the system contains no load. After successful synchronization, the load is abruptly added at  $t = 300$  ms. As shown in Fig. 9, the voltage stays within  $\pm 5\%$  of the rated value in steady state.

A second simulation was conducted to demonstrate synchronization in the presence of the load (in other words, the load is connected at  $t = 0$  s). Given the same initial conditions as above, Fig. 8 illustrates the trajectories of the oscillator state variables (only 10 out of 100 waveforms are shown for clarity). The inductor current within the oscillator  $RLC$  circuit is denoted as  $i_L$ . As shown in Fig. 8, the state-variables reach a stable limit cycle.

*Case Study II (Simulation):* All parameters, except  $R_{net}$ , were reused. The value of  $R_{net}$  was reduced such that  $\|\mathcal{F}(z_{osc}(j\omega), z_{net}^{-1}(j\omega))\|_{\infty} \sigma = 2.78 \not< 1$ , and synchronization is not guaranteed. As illustrated in Fig. 10, the inverters do not synchronize.

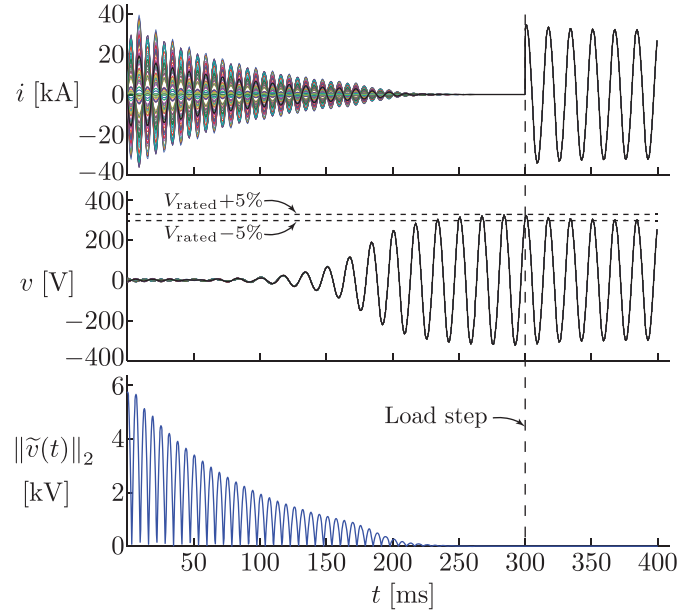


Fig. 9. Inverter output currents, voltages, and voltage synchronization error in the case when  $\|\mathcal{F}(z_{osc}(j\omega), z_{net}^{-1}(j\omega))\|_{\infty} \sigma < 1$ .

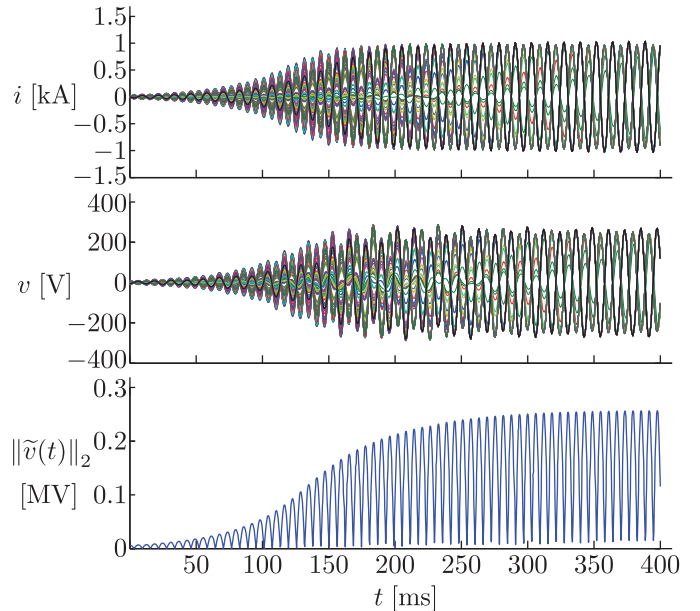


Fig. 10. Inverter output currents, voltages, and voltage synchronization error when  $\|\mathcal{F}(z_{osc}(j\omega), z_{net}^{-1}(j\omega))\|_{\infty} \sigma > 1$  and synchronization is not guaranteed.

*Case Study III (Experimental):* We have built a hardware prototype comprising three parallel H-bridge inverters and a resistive load. A schematic of the experimental hardware setup is given in Fig. 11. The switches in the schematic are N-channel power MOSFETs. Each inverter is rated to deliver 50 W and supplied by a 100 V dc voltage source at the input. The controllers in Fig. 11 regulate the switching action such that each inverter behaves like a dead-zone oscillator. Corresponding parameters in Table I were selected such that the system oscillates at 60 Hz while maintaining a  $60 \text{ V} \pm 5\%$  RMS voltage for all load conditions. Furthermore, synchronization is guaranteed since  $\|\mathcal{F}(z_{osc}(j\omega), z_{net}^{-1}(j\omega))\|_{\infty} \sigma = 0.93 < 1$ . Fig. 12 shows the output currents and load voltages during startup with a 72 W load. The oscillator capacitor voltages were initialized to



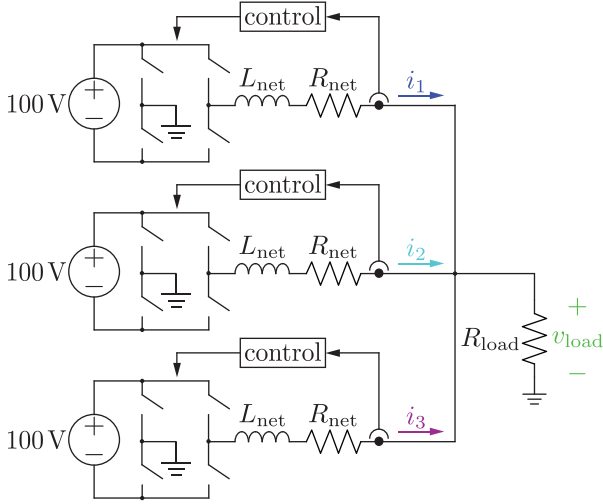


Fig. 11. Schematic of the electrical circuit in the experimental setup.

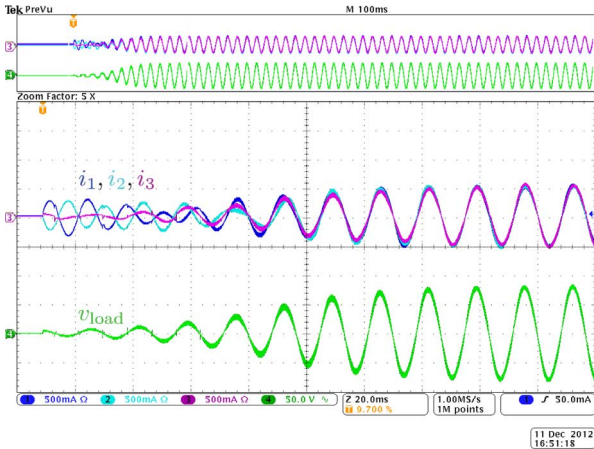


Fig. 12. Oscilloscope screenshot for measured inverter output currents and load voltage.

$v(0) = [5 \text{ V}, 4 \text{ V}, 3 \text{ V}]^T$  within each controller to demonstrate synchronization in spite of non-identical initial conditions.

## VI. CONCLUDING REMARKS AND DIRECTIONS FOR FUTURE WORK

A synchronization condition for nonlinear oscillators coupled through a symmetric LTI network was derived. The condition was shown to be independent of the number of oscillators and the load parameters. We also proposed that parallel inverters in a microgrid be controlled to act as dead-zone oscillators. The resulting microgrid design is modular and does not require communication between inverters. Simulation and experimental results were used to substantiate the analytical results and illustrate the merit of the proposed application.

An important direction for future work is to extend the method presented to address synchronization in three-phase

inverters with constant-power loads. Additionally, synchronization in other network topologies can be investigated with the general approach that we have outlined in this work. Finally, the power quality delivered to the load needs to be investigated by studying the impact of oscillator parameters on the harmonic content in the inverter output waveforms.

## APPENDIX

### A. Derivation of $Y(s)$ in (16)

Diagonalizing  $\mathbf{1}\mathbf{1}^T = P\Xi P^T$ , we can express (15) as follows:

$$\begin{aligned} Y^{-1}(s) &= z_{\text{net}}(s)I_N + z_{\text{load}}(s)P\Xi P^T \\ &= z_{\text{net}}(s)P \left( I_N + \frac{z_{\text{load}}(s)}{z_{\text{net}}(s)}\Xi \right) P^T. \end{aligned} \quad (56)$$

It is easy to show that  $\Xi = \text{diag}\{0, \dots, 0, N\} \in \mathbb{R}^{N \times N}$ . Substituting this in (56), we then obtain

$$Y^{-1}(s) = z_{\text{net}}(s)P \text{diag} \left\{ 1, \dots, 1, 1 + \frac{z_{\text{load}}(s)}{z_{\text{net}}(s)}N \right\} P^T. \quad (57)$$

Inverting (57), we get

$$Y(s) = \frac{1}{z_{\text{net}}(s)}P \text{diag} \left\{ 1, \dots, 1, \frac{1}{1 + \frac{z_{\text{load}}(s)}{z_{\text{net}}(s)}N} \right\} P^T. \quad (58)$$

From the definition of  $z_{\text{eq}}(s)$  in (17), we can write

$$\begin{aligned} Y(s) &= \frac{1}{z_{\text{net}}(s)}P \text{diag} \left\{ 1, \dots, 1, 1 - \frac{z_{\text{load}}(s)}{z_{\text{net}}(s)}N \right\} P^T \\ &= \frac{1}{z_{\text{net}}(s)}P \left( I_N - \frac{z_{\text{load}}(s)}{z_{\text{eq}}(s)}\Xi \right) P^T. \end{aligned} \quad (59)$$

This can be simplified as follows:

$$\begin{aligned} Y(s) &= \frac{1}{z_{\text{net}}(s)z_{\text{eq}}(s)}P(z_{\text{eq}}(s)I_N - z_{\text{load}}(s)\Xi)P^T \\ &= \frac{1}{z_{\text{net}}(s)z_{\text{eq}}(s)} \left( (z_{\text{net}}(s)I_N + N z_{\text{load}}(s))I_N - z_{\text{load}}(s)\mathbf{1}\mathbf{1}^T \right) \\ &= \frac{1}{z_{\text{net}}(s)z_{\text{eq}}(s)} (z_{\text{net}}(s)I_N + z_{\text{load}}(s)(NI_N - \mathbf{1}\mathbf{1}^T)) \\ &= \frac{1}{z_{\text{net}}(s)z_{\text{eq}}(s)} (z_{\text{net}}(s)I_N + z_{\text{load}}(s)\Gamma), \end{aligned} \quad (60)$$

where in the last line, we have used the definition of  $\Gamma$  from (5). Notice that (60) is in the same form as (16), with  $\alpha(s)$  and  $\beta(s)$  given in (17).

### B. Parameters for Simulations and Experiments

The inverter and electrical network parameters used in the simulation and experimental case studies are given in Table I.

TABLE I  
SYSTEM PARAMETERS USED IN THE CASE STUDIES

	Case Study I, II Simulation	Case Study III Experiment
$N$	100	3
$R$	8.66 $\Omega$	95.46 $\Omega$
$L$	433.2 $\mu\text{H}$	4.77 mH
$C$	16.2 mF	1.47 mF
$\sigma$	1.15 S	104.8 mS
$\varphi$	146.1 V	39.8 V
$\epsilon$	0.17	0.17
$R_{\text{net}}$	0.1 $\Omega$ , 0.02 $\Omega$	1 $\Omega$
$L_{\text{net}}$	500 $\mu\text{H}$	6 mH
$R_{\text{load}}$	91.96 m $\Omega$	50 $\Omega$

### C. Heterogeneous Oscillators and Nonidentical Branch Impedances

For real-world microgrid applications, it is unlikely that the branch impedances of the network are identical, and the oscillators (inverters) are homogeneous. However, we can incorporate these sources of uncertainty in the synchronization condition straightforwardly.

First, we attempt to give conditions under which small differences among oscillators leads to small synchronization errors. Towards this end, replace the matrix  $Z_{\text{osc}}(s)$  with  $Z_{\text{osc}}(s) = \bar{Z}_{\text{osc}}(s) + \Delta(s) = \bar{z}_{\text{osc}}(s)I + \Delta(s)$ , where  $\bar{z}_{\text{osc}}(s)$  represents the nominal oscillator impedance and  $\Delta(s)$  is a diagonal matrix that captures deviations of each actual oscillator impedance from the nominal value. With this setup, (25) is modified to

$$\tilde{v}(s) = \mathcal{F}(\bar{Z}_{\text{osc}}(s), Y(s))\tilde{i}_{\text{src}}(s) + e(s), \quad (61)$$

where  $e(s) = \Pi\Delta(s)(\tilde{i}_{\text{src}}(s) - Y(s)v(s))$ . Combining (61) with the nonlinear subsystem  $g(\cdot)$ , we find that if the condition  $\|\mathcal{F}(\bar{Z}_{\text{osc}}(s), Y(s))\|_2\sigma < 1$  (which follows from Theorem 1), is satisfied, then the feedback combination of (61) with  $\tilde{i}_{\text{src}} = -\tilde{g}(\tilde{v})$  will synchronize when  $e(s) \equiv 0$ . Furthermore, taking the  $\mathcal{L}_\infty$  norm of both sides of (61)

$$\|\tilde{v}\|_{\mathcal{L}_\infty} \leq \|\mathcal{F}(\bar{Z}_{\text{osc}}, Y)\|_{\mathcal{L}_1}\|\tilde{i}_{\text{src}}\|_{\mathcal{L}_\infty} + \|e\|_{\mathcal{L}_\infty} + \eta, \quad (62)$$

for some constant  $\eta$  that depends on initial conditions. In addition, recall that the nonlinear subsystem is such that  $\|\tilde{i}_{\text{src}}\|_{\mathcal{L}_\infty} \leq \sigma\|\tilde{v}\|_{\mathcal{L}_\infty}$ . Using the same small-gain argument employed in the case of identical oscillators, the synchronization error in  $\tilde{v} \in \mathcal{L}_\infty$  if network solutions are bounded such that  $e \in \mathcal{L}_\infty$  and if  $\|\mathcal{F}(\bar{Z}_{\text{osc}}, Y)\|_{\mathcal{L}_1}\sigma < 1$  since this would guarantee

$$\|\tilde{v}\|_{\mathcal{L}_\infty} \leq \frac{\|e\|_{\mathcal{L}_\infty} + \eta}{1 - \|\mathcal{F}(\bar{Z}_{\text{osc}}, Y)\|_{\mathcal{L}_1}\sigma} < \infty. \quad (63)$$

In other words, for a network of inverters with different  $z_{\text{osc}}(s)$ , the maximal synchronization error over all time will be upper bounded so long as the small gain condition  $\|\mathcal{F}(\bar{Z}_{\text{osc}}, Y)\|_{\mathcal{L}_1}\sigma < 1$  holds, and all network signals are bounded. Further, this bound will be governed by the maximum value of  $e$  over time, according to the relation (63). Since  $e$  depends directly on  $\Delta(s)$  (which quantifies the differences between network nodes), smaller  $\Delta(s)$  will reduce the maximal asymptotic synchronization error in  $\tilde{v}$  to the extent that if  $\Delta(s)$  is equal to the zero matrix, this error will also reduce to zero, retrieving the original result of Theorem 1.

Now consider that the branch impedances are not identically equal to  $z_{\text{net}}(s) \in \mathbb{C}$ , but for the system of  $N$  inverters, they are given by the vector  $z_{\text{net}}(s) = [z_{\text{net}1}(s), \dots, z_{\text{net}N}(s)]^T \in \mathbb{C}^N$ . For the  $m^{\text{th}}$  branch impedance, we will denote  $z_{\text{net}m}(s) = \kappa_m \bar{z}_{\text{net}}(s)$ , where  $\kappa_m \in \mathbb{R}$ , and  $\bar{z}_{\text{net}}(s)$  is some nominal branch impedance. We will also find it useful to define the vector  $\kappa = [\kappa_1^{-1}, \dots, \kappa_N^{-1}]^T \in \mathbb{R}^N$ . In this case, with reference to Fig. 7, we would design the controller for the  $m$ -th inverter to extract the current  $\kappa_m i_m$ . With this setup, it is straightforward to show that the admittance matrix is given by  $Y(s) = \hat{\alpha}(s)I_N + \hat{\beta}(s)\Gamma$ , where  $\hat{\alpha}(s) = (\bar{z}_{\text{net}}(s) + N\xi)^{-1} =: \hat{z}_{\text{eq}}^{-1}(s)$  and  $\hat{\beta}(s) = \xi(\bar{z}_{\text{net}}(s)\hat{z}_{\text{eq}}(s))^{-1}$ , with  $\xi = z_{\text{load}}(s)(\kappa^T i(s))/(1^T i(s))$ . Using this admittance matrix and applying the same analysis in Theorem 1, we get the synchronization condition:

$$\sup_{\omega \in \mathbb{R}} \left\| \frac{\bar{z}_{\text{net}}(j\omega)z_{\text{osc}}(j\omega)}{\bar{z}_{\text{net}}(j\omega) + z_{\text{osc}}(j\omega)} \right\|_2 \sigma < 1. \quad (64)$$

### ACKNOWLEDGMENT

The authors would like to thank Professor Guy-Bart Stan for some helpful discussions.

### REFERENCES

- [1] C. Liu, D. R. Weaver, S. H. Strogatz, and S. M. Reppert, "Cellular construction of a circadian clock: Period determination in the suprachiasmatic nuclei," *Cell*, vol. 91, pp. 855–860, Dec. 1997.
- [2] J. Pantaleone, "Stability of incoherence in an isotropic gas of oscillating neutrinos," *Phys. Rev. D*, vol. 58, p. 073002, Aug. 1998.
- [3] L. Chua, "Passivity and complexity," *IEEE Trans. Circuits Syst. I, Fundam. Theory Appl.*, vol. 46, pp. 71–82, Jan. 1999.
- [4] S. H. Strogatz, *Nonlinear Dynamics and Chaos: With Applications to Physics, Biology, Chemistry, and Engineering*. Boulder, CO, USA: Westview Press, 2001.
- [5] F. Varela, J. P. Lachaux, E. Rodriguez, and J. Martinerie, "The brainweb: Phase synchronization and large-scale integration," *Nat. Rev. Neurosci.*, vol. 2, pp. 229–239, Apr. 2001.
- [6] C.-X. Fan, G.-P. Jiang, and F.-H. Jiang, "Synchronization between two complex dynamical networks using scalar signals under pinning control," *IEEE Trans. Circuits Syst. I, Fundam. Theory Appl.*, vol. 57, pp. 2991–2998, Nov. 2010.
- [7] F. Dörfler and F. Bullo, "Exploring synchronization in complex oscillator networks," in *Proc. IEEE Conf. Decision Control*, Maui, HI, USA, Dec. 2012, pp. 7157–7170.
- [8] A. Pogromsky and H. Nijmeijer, "Cooperative oscillatory behavior of mutually coupled dynamical systems," *IEEE Trans. Circuits Syst. I, Fundam. Theory Appl.*, vol. 48, pp. 152–162, Feb. 2001.
- [9] G.-B. Stan, "Global analysis and synthesis of oscillations: A dissipativity approach," Ph.D. thesis, Univ. Liege, Liege, Belgium, May 2005.
- [10] M. Arcak, "Passivity as a design tool for group coordination," *IEEE Trans. Autom. Control*, vol. 52, pp. 1380–1390, Aug. 2007.
- [11] G.-B. Stan and R. Sepulchre, "Analysis of interconnected oscillators by dissipativity theory," *IEEE Trans. Autom. Control*, vol. 52, pp. 256–270, Feb. 2007.
- [12] A. Hamadeh, G.-B. Stan, R. Sepulchre, and J. Goncalves, "Global state synchronization in networks of cyclic feedback systems," *IEEE Trans. Autom. Control*, vol. 57, pp. 478–483, Feb. 2012.
- [13] L. A. B. Tôres, J. P. Hespanha, and J. Moehlis, "Power supplies synchronization without communication," in *Proc. Power Energy Soc. Gen. Meet.*, Jul. 2012.
- [14] A. Hamadeh, G.-B. Stan, and J. Goncalves, "Constructive synchronization of networked feedback systems," in *Proc. IEEE Conf. Decision Control*, Dec. 2010, pp. 6710–6715.
- [15] A. Hamadeh, "Constructive robust synchronization of networked control systems," Ph.D. thesis, Cambridge University, Cambridge, U.K., Jun. 2010.
- [16] A. Dhawan, A. Hamadeh, and B. Ingalls, "Designing synchronization protocols in networks of coupled nodes under uncertainty," in *Proc. Amer. Control Conf.*, Jun. 2012, pp. 4945–4950.
- [17] R. Lasseter, "Microgrids," in *Proc. IEEE Power Eng. Soc. Winter Meet.*, 2002, vol. 1, pp. 305–308.

- [18] J. Lopes, C. Moreira, and A. Madureira, "Defining control strategies for microgrids islanded operation," *IEEE Trans. Power Syst.*, vol. 21, pp. 916–924, May 2006.
- [19] J. Vasquez, J. Guerrero, A. Luna, P. Rodriguez, and R. Teodorescu, "Adaptive droop control applied to voltage-source inverters operating in grid-connected and islanded modes," *IEEE Trans. Ind. Electron.*, vol. 56, pp. 4088–4096, Oct. 2009.
- [20] A. Mohd, D. Ortjohann, and O. Omari, "Review of control techniques for inverters parallel operation," *Elect. Power Syst. Res.*, vol. 80, pp. 1477–1487, Dec. 2010.
- [21] D. Logue and P. Krein, "Preventing instability in dc distribution systems by using power buffering," in *Proc. IEEE Power Electron. Specialists Conf.*, 2001, vol. 1, pp. 33–37.
- [22] F. Katiraei, M. Irvani, and P. Lehn, "Small-signal dynamic model of a micro-grid including conventional and electronically interfaced distributed resources," *IET Gener., Transm., Distrib.*, vol. 1, pp. 369–378, May 2007.
- [23] B. Johnson, A. Davoudi, P. Chapman, and P. Sauer, "Microgrid dynamics characterization using the automated state model generation algorithm," in *IEEE Proc. Int. Symp. Circuits Syst.*, Jun. 2010, pp. 2758–2761.
- [24] B. Johnson, A. Davoudi, P. Chapman, and P. Sauer, "A unified dynamic characterization framework for microgrid systems," *Elect. Power Compon. Syst.*, vol. 40, pp. 93–111, Nov. 2011.
- [25] P. Piagi and R. Lasseter, "Autonomous control of microgrids," in *Proc. IEEE Power Eng. Soc. Gen. Meet.*, Jun. 2006, vol. 6, pp. 1–8.
- [26] Q.-C. Zhong, "Robust droop controller for accurate proportional load sharing among inverters operated in parallel," *IEEE Trans. Ind. Electron.*, vol. 60, pp. 1281–1290, Apr. 2013.
- [27] P. T. Krein, *Elements of Power Electronics*. New York: Oxford Univ. Press, 1998.
- [28] F. Katiraei and M. Irvani, "Power management strategies for a micro-grid with multiple distributed generation units," *IEEE Trans. Power Syst.*, Nov. 2006.
- [29] E. Furtado, L. Aguirre, and L. Tôrres, "UPS parallel balanced operation without explicit estimation of reactive power: A simpler scheme," *IEEE Trans. Circuits Syst. II, Exp. Briefs*, vol. 55, pp. 1061–1065, Oct. 2008.
- [30] J. W. Simpson-Porco, F. Dörfler, and F. Bullo, "Droop-controlled inverters are Kuramoto oscillators," in *Proc. 3rd IFAC Workshop Distrib. Estimation Control Netw. Syst.*, Sep. 2012, pp. 264–269.
- [31] J. W. Simpson-Porco, F. Dörfler, and F. Bullo, "Synchronization and power sharing for droop-controlled inverters in islanded microgrids," *Automatica*, vol. 49, no. 9, pp. 2603–2611, Sep. 2013.
- [32] J. W. Simpson-Porco, F. Dörfler, Q. Shafiee, J. M. Guerrero, and F. Bullo, "Stability, power sharing, and distributed secondary control in droop-controlled microgrids," in *Proc. IEEE Int. Conf. Smart Grid Commun.*, Vancouver, BC, Canada, Oct. 2013, to be published.
- [33] A. Van der Schaft, "Lecture Notes in Control and Information Sciences," in *L2-Gain and Passivity Techniques in Nonlinear Control*. London, U.K.: Springer, 1996.
- [34] H. Khalil, *Nonlinear Systems*, 3rd ed. Upper Saddle River, NJ, USA: Prentice-Hall, 2002.
- [35] L. B. Cremean and R. M. Murray, "Stability analysis of interconnected nonlinear systems under matrix feedback," in *Proc. IEEE Conf. Decision Control*, Dec. 2003, vol. 3, pp. 3078–3083.
- [36] R. Olfati-Saber and R. M. Murray, "Consensus problems in networks of agents with switching topology and time-delays," *IEEE Trans. Autom. Control*, vol. 49, pp. 1520–1533, Sep. 2004.
- [37] J. Guerrero, L. de Vicuna, J. Matas, M. Castilla, and J. Miret, "A wireless controller to enhance dynamic performance of parallel inverters in distributed generation systems," *IEEE Trans. Power Electron.*, vol. 19, pp. 1205–1213, Sep. 2004.
- [38] K. Zhou, J. Doyle, and K. Glover, *Robust and Optimal Control*. Upper Saddle River, NJ, USA: Prentice-Hall, 1996.



**Brian B. Johnson** (S'08–M'13) received the B.S. degree in physics from Texas State University, San Marcos, TX, USA, in 2008. He received the M.S. and Ph.D. degrees in electrical and computer engineering from the University of Illinois at Urbana-Champaign, IL, USA, in 2010 and 2013, respectively.

He is currently an Electrical Engineer with the National Renewable Energy Laboratory in Golden, CO, USA. He was awarded a National Science Foundation Graduate Research Fellowship in 2010. His research interests are in power electronics, distributed generation, renewable energy systems, and nonlinear controls.



**Sairaj V. Dhople** (S'09–M'13) received the B.S., M.S., and Ph.D. degrees in electrical engineering, in 2007, 2009, and 2012, respectively, from the University of Illinois at Urbana-Champaign, IL, USA.

He is currently an Assistant Professor in the Department of Electrical and Computer Engineering at the University of Minnesota (Twin Cities), MN, USA, where he is affiliated with the Power and Energy Systems research group. His research interests include modeling, analysis, and control of power electronics and power systems with a focus on renewable integration.



**Abdullah O. Hamadeh** obtained his M.Eng., M.A., and Ph.D. degrees in electrical engineering from the University of Cambridge, Cambridge, U.K., in 2005, 2008, and 2010 respectively. His doctoral research was in the control and synchronization of networked dynamical systems.

Between 2010 and 2013 he held postdoctoral positions at the University of Waterloo and at Rutgers University, and he is currently a Postdoctoral Associate at the Department of Mechanical Engineering at the Massachusetts Institute of Technology, Cambridge, MA, USA. His current research interests are in the applications of control theoretic techniques to systems and synthetic biology and in the control of electrical power networks.



**Philip T. Krein** (S'76–M'82–SM'93–F'00) received the B.S. degree in electrical engineering and the A.B. degree in economics and business from Lafayette College, Easton, PA, USA, and the M.S. and Ph.D. degrees in electrical engineering from the University of Illinois, Urbana, IL, USA.

He was an Engineer with Tektronix in Beaverton, OR, USA, then returned to the University of Illinois at Urbana-Champaign. Currently, he holds the Grainger Endowed Director's Chair in Electric Machinery and Electromechanics as Professor and Director of the Grainger Center for Electric Machinery and Electromechanics, Department of Electrical and Computer Engineering. He published an undergraduate textbook, *Elements of Power Electronics* (Oxford, U.K.: Oxford Univ. Press, 1998). In 2001, he helped initiate the IEEE International Future Energy Challenge, a major student competition involving fuel cell power conversion and energy efficiency. He holds 26 U.S. patents with additional patents pending. His research interests address all aspects of power electronics, machines, drives, and electrical energy, with emphasis on nonlinear control and distributed systems.

Dr. Krein is a Registered Professional Engineer in the States of Illinois and Oregon. He was a senior Fulbright Scholar at the University of Surrey, Surrey, U.K. and was recognized as a University Scholar, the highest research award at the University of Illinois. In 2003, he received the IEEE William E. Newell Award in Power Electronics. He is a past president of the IEEE Power Electronics Society, and served as a member of the IEEE Board of Directors. In 2005–2007, he was a Distinguished Lecturer for the IEEE Power Electronics Society. In 2008, he received the Distinguished Service Award from the IEEE Power Electronics Society. He is an Associate Editor of the IEEE TRANSACTIONS ON POWER ELECTRONICS and serves as Academic Advisor for the Department of Electronic and Information Engineering at Hong Kong Polytechnic University. He is a founder and Director of SolarBridge Technologies, a developer of long-life integrated solar energy systems.